

MODELING A HOLLOW MICRO-PARTICLE PRODUCTION PROCESS

V. S. Shabde, S. V. Emets, U. Mann, and K. A. Hoo*
Department of Chemical Engineering
Texas Tech University, Lubbock, TX 79409-3121

N. Carlson and G. Gladysz
Los Alamos National Laboratories
Los Alamos, NM 87545

January 28, 2005

Abstract

The process to be modeled produces micro-hollow particles based on spray drying technology. This process involves droplet formation, solvent(s) evaporation, formation of the impermeable outer layer, and decomposition of the blowing agent. The objective of this work is to develop a fundamental model that describes the formation of the hollow particles starting from a single droplet. This model is then used to predict the time to skin formation in the presence of parameter uncertainties and varying operating conditions.

1 Introduction

Hollow spherical particles have been used in a large number of applications in diverse fields. One of the most important application is the use of hollow micro-particles (also referred to as *microballoons*) as fillers in syntactic foams. The hollow particles provide a means to tailor the manufacture of light materials (foams) with desirable mechanical, thermal, and electrical properties that are easily molded and machined due to the small size of the particles.

The properties of the hollow particles affect the properties of the syntactic foams – most notably, the density of the particles and their mechanical properties. Both of these properties depend mainly on three factors: (i) the type of material (polymer), (ii) the diameter of the particles, and (iii) the thickness of the skin. For a given particle diameter,

*Author to whom all correspondence should be sent, k.hoo@coe.ttu.edu, ph.: (806)742-4079, fax: (806)742-3552

the thinner the particle skin, the smaller the particle density. Mechanical properties depend on the rigidity and thickness of the skin. It is essential to produce reliably and economically micro-hollow polymeric particles with the desirable properties. To date, there are three main methods to produce hollow micro-particles [1]: (i) Spray-drying based process; (ii) sacrificial core method; and (iii) emulsion and phase separation techniques. The most widely used industrial process is based on spray-drying technology. In this process, a polymer solution (the material of the particle) is atomized in a spray-drying chamber. This solution also contains a latent gas (blowing agent), which, as described below, leads to the formation of the hollow core. As the droplets are exposed to the hot air, the solvent evaporates forming a layer of higher concentration of polymer at the outer boundary of the particle. As the particle continues to shrink an impermeable layer is formed. Upon completion of the solvent evaporation, the temperature of the droplet (now a particle) rises, causing the decomposition of the blowing agent trapped in the center of the particle; thus forming the hollow core.

The objective of this work is to develop a physics-based model of the process to determine the best or optimum operating conditions that will produce hollow particles with desirable properties. The literature does not provide a fundamental model that describes the process of producing hollow micro-particles. A large volume of work has been carried out on the modeling of conventional spray drying operations (formation of non-hollow particles) [2], mainly as they apply in the food industry. However, these models do not apply to the production of hollow particles because they do not account for the formation of an impermeable skin and generation of gas in the core. This work is aimed at the development and verification of a fundamental model that describes the production of hollow micro particles.

The paper is organized as follows. Section 2 briefly describes the experimental system. Next, the model formulation is described and developed. Section 4 then outlines a numerical approach that uses the method of Gradient Weighted Moving Finite Elements to solve a system of partial differential equations (PDEs) with a moving boundary. The results and discussion of results are provided in section 5. Lastly, section 6 summarizes the work presented.

2 Experimental System

The experimental system is constructed to produce hollow micro-polymeric particles. The experimental unit, shown in Figure 1, consists of five major systems: a hot air delivery system, a liquid delivery system, an atomizer, a drying chamber, and a particle collection system (cyclone and filter). The experimental system has the following features:

1. A maximum inlet air temperature of 1000°F
2. A peristaltic pump to adjust the flow rate of the polymer solution.
3. An atomizer to generate the droplets (range of 10 to 60 μ).

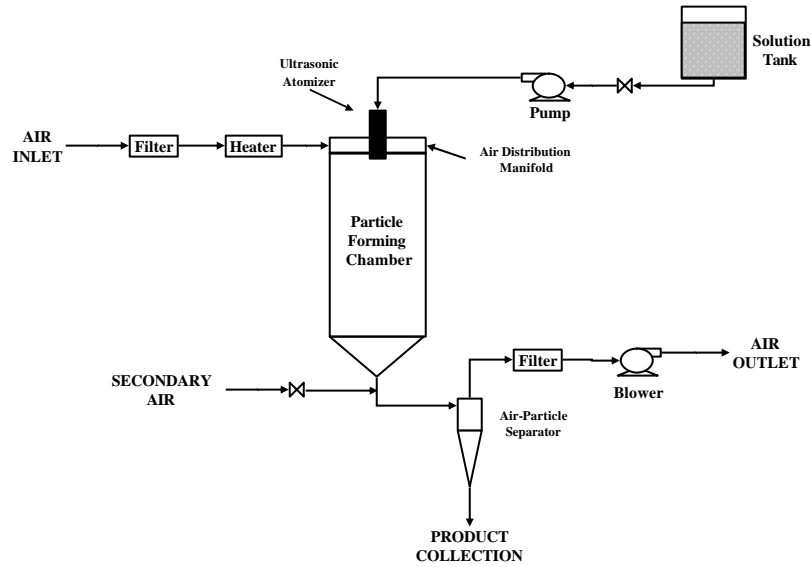


Figure 1: Schematic diagram of the experimental system.

4. A cyclone and a filter to collect the particles.
5. A secondary ambient air flow to regulate the exit temperature to protect the blower.

Figure 2 shows samples of the hollow micro-particles produced by the experimental system. These hollow micro-particles are spherical in shape with impermeable skins with thicknesses *on the average* of 2 to 3 μ . The mean particle diameters are between 50 to 100 μ .

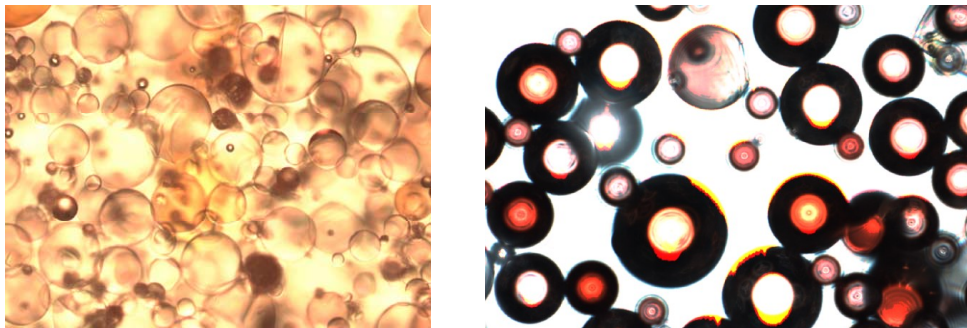


Figure 2: Hollow micro-particles made using the experimental system. Left panel: thin skin. Right panel: thick skin.

3 Modeling a Single Droplet

The first step in the formulation of the model is to describe the formation of a single hollow particle. Non-steady state energy and mass balances over a droplet lead to a system of two non-linear parabolic partial differential equations (PDEs). Because the droplet shrinks this is a moving boundary problem, which negates the use of typical PDE numerical solvers to obtain a solution. To solve this nonlinear system of PDEs a moving finite element method [3] is applied.

3.1 Physical phenomena

Consider a single droplet; a number of different phenomena occur as it passes through the chamber. Since the air is at a higher temperature than the droplet, heat is convected to the droplet. This heat is conductively transferred from the surface of the droplet toward the interior thus increasing the temperature inside the droplet. When the surface temperature reaches the boiling temperature of solvent, evaporation of solvent begins to occur at the surface. Thus, the droplet passes through two steps: a heating step where sensible heat is supplied to the droplet to raise its temperature to the evaporation temperature *and* an evaporation step. In the latter step, the heat supplied is used (a) to provide the latent heat to evaporate the solvent and (b) to provide the sensible heat which is conducted into the core of the droplet.

Solvent vapors are released to the bulk air. The driving force for this transfer is provided by the difference in the concentration of solvent at the droplet surface and the surrounding air. Similarly, the evaporation of the solvent provides a driving force for the diffusion of the solvent from the interior of the particle to the surface of the particle.

As the solvent evaporates, the droplet shrinks. Because of a lower polymer mobility, the polymer concentration near the surface increases. This phenomenon is known as *skinning* [4]. Thus, the polymer concentration gradient at the surface is steeper as compared to the profile (flat) away from the surface (interior to the particle). A sufficiently high heating rate can evaporate almost all the water leaving only polymer at the surface that forms the impermeable shell.

3.2 Model assumptions

The formation of a hollow particle is divided into two steps: (a) evaporation of the solvent (shrinking) and (b) decomposition of the trapped blowing agent. Figure 3 represents an illustration of the mechanisms and the temperature and concentration profiles during droplet evaporation. In this work, the solvent is water. It is assumed that as the droplet temperature reaches the evaporation temperature of the water, the polymer diffuses to the surface. Once all the water is evaporated, the latent gas (blowing agent) that was trapped inside the particle decomposes, thus forming a shell.

The following assumptions are made in the development of the model:

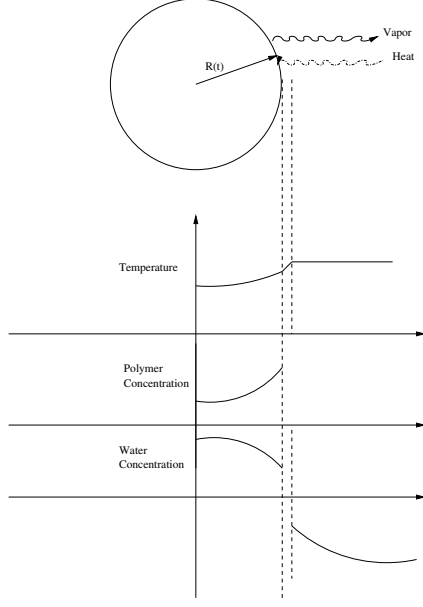


Figure 3: Temperature and concentration profiles during droplet evaporation.

1. Because of the relatively large amount of hot air, it is assumed that the conditions of the hot air do not vary with time. Hence, variations in the air conditions are omitted from the model.
2. A spherically symmetric field exists in and around the droplet. Thus, internal circulation is absent. This is reasonable since the droplets are small.
3. There is negligible relative velocity between the droplet and the air. Hence, the external heat and mass transfers are approximated by conduction and diffusion, respectively.

3.3 Model formulation

Material and energy balances are made about a spherical shell element of the droplet. The heat transferred to the interior of the droplet from the surface is transferred by conduction. This leads to the following equation and the corresponding boundary condition at the center of the droplet arising due to symmetry of the droplet. Thus,

$$\frac{\partial(\rho C_p T)}{\partial t} = \frac{1}{r^2} \frac{\partial}{\partial r} \left(k r^2 \frac{\partial T}{\partial r} \right) \quad 0 \leq r \leq R(t), t > 0$$

where T is temperature, k is the thermal conductivity, ρ is the density of the solution, C_p is the specific heat capacity of the solution, and the independent variables are time, t , and radial distance, r . It is assumed that k is independent of the radial position and time; thus the above equation becomes,

$$\frac{\partial(T)}{\partial t} = \alpha \frac{1}{r^2} \frac{\partial}{\partial r} \left(r^2 \frac{\partial T}{\partial r} \right) \quad 0 \leq r \leq R(t), t > 0 \quad (1)$$

where $\alpha = k/\rho C_p$ is the thermal diffusivity. Initially, the particle temperature profile is uniform when the droplet enters the spraying chamber thus, the corresponding initial condition is given by,

$$T(r, 0) = T_0 \quad 0 \leq r \leq R \quad (2)$$

A species balance on the polymer is given by,

$$\frac{\partial(c_P)}{\partial t} = \mathcal{D} \frac{1}{r^2} \frac{\partial}{\partial r} \left(r^2 \frac{\partial c_P}{\partial r} \right) \quad 0 \leq r \leq R(t) \quad (3)$$

with initial condition,

$$c_P(r, 0) = c_{P,0}$$

where the binary diffusion coefficient \mathcal{D} of the polymer and water is assumed to be independent of the radial position and time, and c_P is the polymer concentration. The initial concentration profiles are assumed to be uniform.

Similarly, a mass balance of the water gives,

$$\frac{\partial(c_W)}{\partial t} = \mathcal{D} \frac{1}{r^2} \frac{\partial}{\partial r} \left(r^2 \frac{\partial c_W}{\partial r} \right) \quad 0 \leq r \leq R(t) \quad (4)$$

with initial condition,

$$c_W(r, 0) = c_{W,0}$$

where c_W is the water concentration.

3.4 Boundary conditions

Since the droplet goes through two steps of heating and evaporation, two sets of boundary conditions are required at the surface. The boundary conditions at the center arise due to the symmetry of the droplet and are unchanged during both steps,

$$\begin{aligned} \frac{\partial T}{\partial r}(0, t) &= 0 & t \geq 0 \\ \frac{\partial c_P}{\partial r}(0, t) &= 0 & t \geq 0 \\ \frac{\partial c_W}{\partial r}(0, t) &= 0 & t \geq 0 \end{aligned} \quad (5)$$

3.4.1 Heating step

An energy balance at the surface provides the boundary condition during the heating step,

$$-k \frac{\partial T}{\partial z}(R, t) = h(T_{air} - T|_R) \quad T|_R < T_{sat} \quad (6)$$

where h is the external heat transfer coefficient, T_{sat} is the evaporation temperature of water and T_{air} is the temperature of the air stream. During this step there is no flux of either water or polymer at the surface of the droplet. Thus,

$$\begin{aligned} \mathcal{D} \frac{\partial c_P}{\partial r} &= 0 & 0 \leq r \leq R(0) \\ \mathcal{D} \frac{\partial c_P}{\partial r} &= 0 & 0 \leq r \leq R(0) \end{aligned} \quad (7)$$

3.4.2 Evaporation step

In the evaporation step, the temperature at the surface is constant at the boiling point of the solvent. In the case of the polymer, a mass conservation on the polymer is used to obtain the boundary condition. Since the polymer does not diffuse out of the droplet, the total amount of polymer in the droplet (M_P) remains constant,

$$M_P = \int_0^{R(t)} c_P r^2 dr \quad (8)$$

Taking the derivative of Eqn. (8) with respect to time gives,

$$\frac{\partial M_P}{\partial t} = \int_0^{R(t)} \frac{\partial c_P}{\partial t} r^2 dr + c_P(R(t), t) R^2(t) \frac{dR(t)}{dt} = 0 \quad (9)$$

where $R(t)$ is the radius of the droplet at time t and $\frac{dR(t)}{dt}$ is the rate of movement of the surface. The solution to Eqn. (9) is given by,

$$\mathcal{D} \frac{\partial c_P}{\partial r} \Big|_{r=R(t)} + c_P \frac{dR(t)}{dt} = 0.$$

The boundary condition for water at the surface is obtained by recognizing that the water losses are proportional to the motion of the surface. Thus, the boundary conditions at the surface are given by,

$$\begin{aligned} T|_{R(t)} &= T_{sat} \\ \mathcal{D} \frac{\partial c_P}{\partial r} \Big|_{r=R(t)} + c_P \frac{dR(t)}{dt} &= 0 \\ \mathcal{D} \frac{\partial c_W}{\partial r} \Big|_{r=R(t)} &= \frac{\rho_W}{\lambda} (h(T|_{R(t)} - T_{air}) - k \frac{\partial T}{\partial r}) \end{aligned} \quad (10)$$

where λ is the heat of vaporization and ρ_W is the density of water.

3.4.3 Surface motion

During the heating step, the radius of the droplet does not vary. However, in the evaporation step, the surface and hence the radius changes with time as water is evaporated. Thus, the radius can be determined from the following equations,

$$\begin{aligned} \text{Heating step: } R(t) &= R(0) & t &\leq t_H \\ \text{Evaporation step: } \frac{dR}{dt} &= \frac{\rho_W}{\lambda} (h(T|_{R(t)} - T_{air}) - k \frac{\partial T}{\partial r}) & t &> t_H \end{aligned} \quad (11)$$

where t_H is the time to reach the evaporation temperature of water.

3.5 Reduction to dimensionless form

To simplify the analysis, it is convenient to reduce the model to dimensionless form. This is done by defining the dimensionless variables given in Table 1, and selecting a characteristic time constant, t_0 given by:

$$t_0 \equiv \frac{R(0)^2}{\mathcal{D}}$$

For definitions of the symbols, the reader is referred to the nomenclature section. The appropriate scaling for length is to use the initial droplet radius in reference to the initial density and the initial driving force. Concentrations and temperature are made dimensionless by using the initial conditions.

Using the variables in Table 1, the dimensionless model and initial conditions are found to be,

$$\begin{aligned} \frac{\partial(\bar{c}_W)}{\partial\tau} &= \frac{1}{x^2} \frac{\partial}{\partial x} (x^2 \frac{\partial \bar{c}_W}{\partial x}) & \bar{c}_W(x, 0) &= \bar{c}_{W,0} \\ \frac{\partial(\bar{c}_P)}{\partial\tau} &= \frac{1}{x^2} \frac{\partial}{\partial x} (x^2 \frac{\partial \bar{c}_P}{\partial x}) & \bar{c}_P(x, 0) &= \bar{c}_{P,0} \\ \frac{\partial\theta}{\partial\tau} &= Le \frac{1}{x^2} \frac{\partial}{\partial x} (x^2 \frac{\partial\theta}{\partial r}) & \theta(x, 0) &= \theta_0 \end{aligned} \quad (12)$$

The dimensionless boundary conditions are given by,

$$\begin{array}{l}
 \text{Center of the droplet} \\
 \text{Heating: the droplet surface}
 \end{array}
 \quad
 \begin{array}{l}
 x = 0 \\
 x = X(\tau) = \frac{R(t)}{R_0}
 \end{array}
 \quad
 \left\{
 \begin{array}{l}
 \frac{\partial \bar{c}_W}{\partial x}(0, \tau) = 0, \quad \tau \geq 0 \\
 \frac{\partial \bar{c}_P}{\partial x}(0, \tau) = 0, \quad \tau \geq 0 \\
 \frac{\partial \theta}{\partial x}(0, \tau) = 0, \quad \tau \geq 0 \\
 \frac{\partial \theta}{\partial x} = Bi_H(\theta_{air} - \theta(R(\tau))) \\
 \frac{\partial \bar{c}_P}{\partial x} = 0 \\
 \frac{\partial \bar{c}_W}{\partial x} = 0
 \end{array}
 \right.
 \quad (13)$$

$$\text{Evaporation: the droplet surface} \quad x = X(\tau) = \frac{R(t)}{R(0)} \quad \left\{
 \begin{array}{l}
 \theta|_{X(\tau)} = \theta_{sat} \\
 \frac{\partial \bar{c}_P}{\partial x} = -\bar{c}_P \frac{dX}{d\tau} \\
 \frac{\partial \bar{c}_W}{\partial x} = (1 - \bar{c}_W) \frac{dX}{d\tau}
 \end{array}
 \right. \quad (14)$$

The surface motion is found from the following expressions,

$$\begin{array}{l}
 \text{Heating step:} \\
 \text{Evaporation step:}
 \end{array}
 \quad
 \begin{array}{l}
 X(\tau) = 1.0 \\
 \frac{dX}{d\tau} = LeH_{evap} \left(Bi_H(\theta_{air} - \theta(X(\tau))) - \frac{\partial \theta}{\partial x} \right)
 \end{array}
 \quad (15)$$

3.6 Model parameters

The parameters that are necessary to solve the above system of equations include the mass diffusivity (binary diffusion coefficient) of the water-polymer mixture, the thermal diffusivity of the mixture, and the external heat (h) and mass (k_x) transfer coefficients. The external heat and mass transfer coefficients are obtained from the following expressions [5],

$$\begin{aligned}
 Nu &= 2 + 0.6 Re^{1/3} Pr^{2/3} \\
 Sh &= 2 + 0.6 Re^{1/3} Sc^{2/3}
 \end{aligned}
 \quad (16)$$

where Re is the Reynolds number, Pr is the Prandtl number, Sc is the Schmidt number, Nu is the Nusselt number, and Sh is the Sherwood number. The Nusselt number is defined as

the ratio of the product of the heat transfer coefficient and the distance over which the heat is transferred, which in this case is the particle diameter (d_p) and the thermal conductivity of the heating medium (k_{air}),

$$Nu \equiv \frac{hd_p}{k_{air}}$$

The Sherwood number is a ratio of the product of the mass transfer coefficient and d_p and the product of the concentration of water at the surface and the binary diffusion coefficient of polymer and water.

$$Sh \equiv \frac{k_x d_p}{c_W \mathcal{D}_{air}}$$

Since the diameter of the droplet is small, the relative velocity between the droplet and the gas (air) is small. It then follows that the Reynolds number is small ($\sim 10^{-2}$). Thus, the values of h and k_x can be found by,

$$\begin{aligned} h &\sim 2 \frac{k_{air}}{d_p} \\ k_x &\sim 2 \frac{c_W \mathcal{D}_{air}}{d_p} \end{aligned} \tag{17}$$

The thermal conductivity of water is estimated from the following expression [6],

$$k = -3.8538 \times 10^{-1} + 5.25 \times 10^{-3}(T) - 6.369 \times 10^{-6}(T)^2$$

where, T is the temperature.

The binary diffusivity of water and polymer is estimated using Wilke and Chang correlation [7]. The parameters, for the experimental conditions used here, are given in Table 2.

4 Numerical Method

To solve the system of equations given in Eqn. (12) with boundary conditions given by Eqn. (13), the method of Gradient Weighted Moving Finite Elements (GWMFE) is used [8]. This is a moving node finite element method that provides a natural framework for solving the evaporation phase of the droplet because the change in the particle size as a function of time and space has to be followed accurately. Another approach to solve the model equations is to employ a change of variables to a normalized coordinate system where the surface position is fixed [9]. However, the complexity of the system of equations is increased because a convection term is added to the model. The GWMFE method is the preferred method in this work not only because it preserves the original form of the model but also because it follows the boundary motion accurately. The following explanation is taken from the work of Miller and Carlson [10].

4.1 Mathematical formulation

Consider a partial differential equation of the form given by,

$$u_t = \mathcal{L}u$$

where \mathcal{L} is a differential operator and u represents a position. Then, the above equation represents the *vertical motion of $u(t)$* . Consider, *normal motion \dot{n}* , where $\dot{n} \equiv u_t / \sqrt{1 + u_x^2}$ and u_x means the partial derivative with respect to position. The above equation can be converted into the normal motion form by dividing by $\sqrt{1 + u_x^2}$,

$$\dot{n} = K(u) \tag{18}$$

Let $U(x, t)$ given by,

$$U(x, t) = \sum_j \beta^j U_j(t) \tag{19}$$

be an approximate solution to the above equation. It then follows that the motion of \dot{U} is given by

$$\dot{U}(x, t) = \sum_j \beta^j \dot{U}_j(t)$$

where β^j are the basis functions. In this work, the set β^j is chosen to be piecewise linear *hat functions*,

$$\beta^j = \begin{cases} \frac{x - x_{j-1}}{x_j - x_{j-1}} & x_{j-1} \leq x \leq x_j \\ \frac{x_{j+1} - x}{x_{j+1} - x_j} & x_j \leq x \leq x_{j+1} \end{cases} \tag{20}$$

Other choices of basis functions can be used, however in this work, higher order basis functions do not increase the accuracy of the solution.

The normal motion with this assumed function is then given by,

$$\dot{n} = \dot{u} \cdot \mathbf{n} = \sum_j \dot{x}_j (\beta^j n_1) + \dot{u}_j (\beta^j n_2)$$

where

$$\mathbf{n} \equiv (n_1, n_2) \equiv \left(1/\sqrt{1 + U_x^2}, U_x/\sqrt{1 + U_x^2} \right)$$

is a unit normal vector, \dot{x}_j are the nodal motions, and \dot{U}_j are the nodal amplitudes (value of approximation ($U(x, t)$) at every node).

4.2 Residual minimization

The solution for U_j is obtained by minimizing the residual, ψ , of Eqn. (18) with respect to the nodal velocities and the nodal amplitudes. The residual is given by,

$$\psi \equiv \int (\dot{n} - K(u))^2 dS$$

and the derivatives with respect to the nodal velocities and amplitudes are given by,

$$\frac{1}{2} \frac{\partial \psi}{\partial \dot{x}_j} = \int (\dot{n} - K(u)) \beta^j n_1 dS$$

$$\frac{1}{2} \frac{\partial \psi}{\partial \dot{U}_j} = \int (\dot{n} - K(u)) \beta^j n_2 dS$$

The result is a system of ordinary differential equations in the independent variable time that can be solved by any initial value problem solver. In this work a modified Newton method is used [10].

5 Results and Discussion

The dimensionless equations are solved using the GWMFE method at design (nominal) conditions ($\theta_{in} = 0$, $\bar{c}_P(0) = 0.192$, $\theta_{air} = 1$, $Bi_H = 0.0938$, $Le = 145.92$, $H_{evap} = 1.97$, and $R(0) = 60\mu$) and at non-nominal conditions. The latter represents the performance of the system to parameter uncertainties and to changes in the operating conditions. In the case of parameter uncertainties, the heat transfer coefficient and the binary diffusion coefficient are varied $\pm 25\%$. In the case of the operating conditions the inlet polymer concentration of the droplet is varied by $\pm 10\%$, the inlet droplet temperature by $\pm 15\%$, and the air temperature by $\pm 8\%$.

Figure 4 shows how the droplet radius, the polymer concentration and the temperature at the surface vary as functions of dimensionless time at the design conditions. From the graph, it is observed that the evaporation temperature is reached at $\tau = 0.005$ dimensionless time units ($t = 0.0144$ s and $t_0 = 2.88$ s). Simultaneously, the surface (\square) of the droplet begins to recede. As the water evaporates, the polymer (\circ) diffuses inside the droplet; the temperature at the surface remains constant at the evaporation temperature. Figure 5 shows the corresponding spatial profiles of the polymer and the water concentrations, respectively. The model predicts the concentration and temperature variations that take place during the operation (*cf* Figure 3).

To study the effect of changes in the heat transfer rate, the heat transfer coefficient is changed by $\pm 15\%$ and $\pm 25\%$ from its nominal value. The resulting polymer concentration profile is shown in Figure 6. From the graph, skin formation is sensitive to the rate of heat transferred. The time for skin formation is defined as the time required for the concentration of the polymer to reach 100% at the surface. The dependence on the amount of heat transferred is non-linear. That is, when the heat transfer coefficient is increased by 15 and 25%, the time for skin formation does not change by the same amount when decreased by the same amount. It is not surprising that beyond a certain point, increasing the heat transfer rate does not affect appreciably the time for skin formation and that decreasing the heat transferred will retard the rate of skin formation.

Similar tests are carried out for changes in the diffusivity coefficient. The polymer concentration profiles are shown in Figure 7.

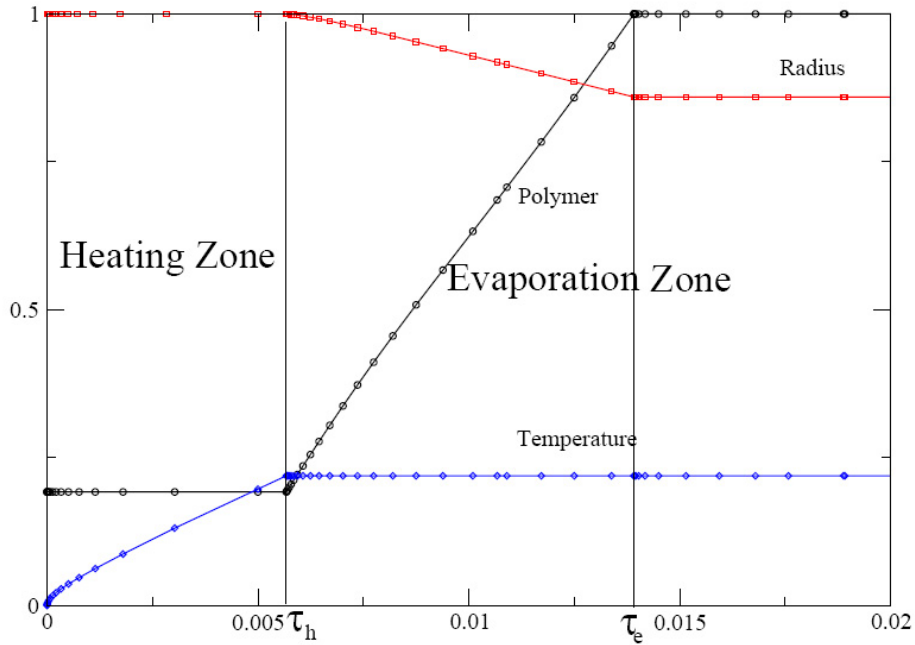


Figure 4: Model predictions at design conditions. The polymer and temperature profiles are those at the surface. \circ : \bar{c}_P (polymer), \diamond : θ (temperature), and \square : X (radius)

From the graph, it is observed that as the diffusion increases, the time required for skin formation decreases. However, since the heat transfer rate is constant, the water does not evaporate at a faster rate and remains on the surface longer delaying the skin formation. Again the relationship between the binary mass diffusivity and the time for skin formation is non-linear with shorter lengths of time when the diffusivity is increased than when the diffusivity is decreased by the same amount.

The inlet concentration of the droplet is varied to investigate its effect on skin formation. For changes of $\pm 10\%$ in the inlet concentration of the polymer there appears to be negligible changes in the thermal and mass transfer characteristics of the droplet. However, it is observed that a decrease in the polymer concentration increases the time required for skin formation. At a given constant heat transfer rate, the time required to evaporate the additional water is increased which in turn results in a longer time for skin formation. The effect of changes in the polymer concentration on the time to skin formation is shown in Figure 8.

The inlet droplet temperature and the gas temperature are varied to study their effect on skin formation. A $\pm 10^\circ\text{C}$ change in the inlet temperature of the droplet did not produce a significant change in the time to skin formation. This indicates that the air supplied is at a sufficiently high temperature to compensate for reasonable changes in the inlet droplet temperature. However, variations in the air temperature have significant effect on the time for skin formation. This is observed when changes of 8% ($\pm 50^\circ\text{C}$) to the air inlet

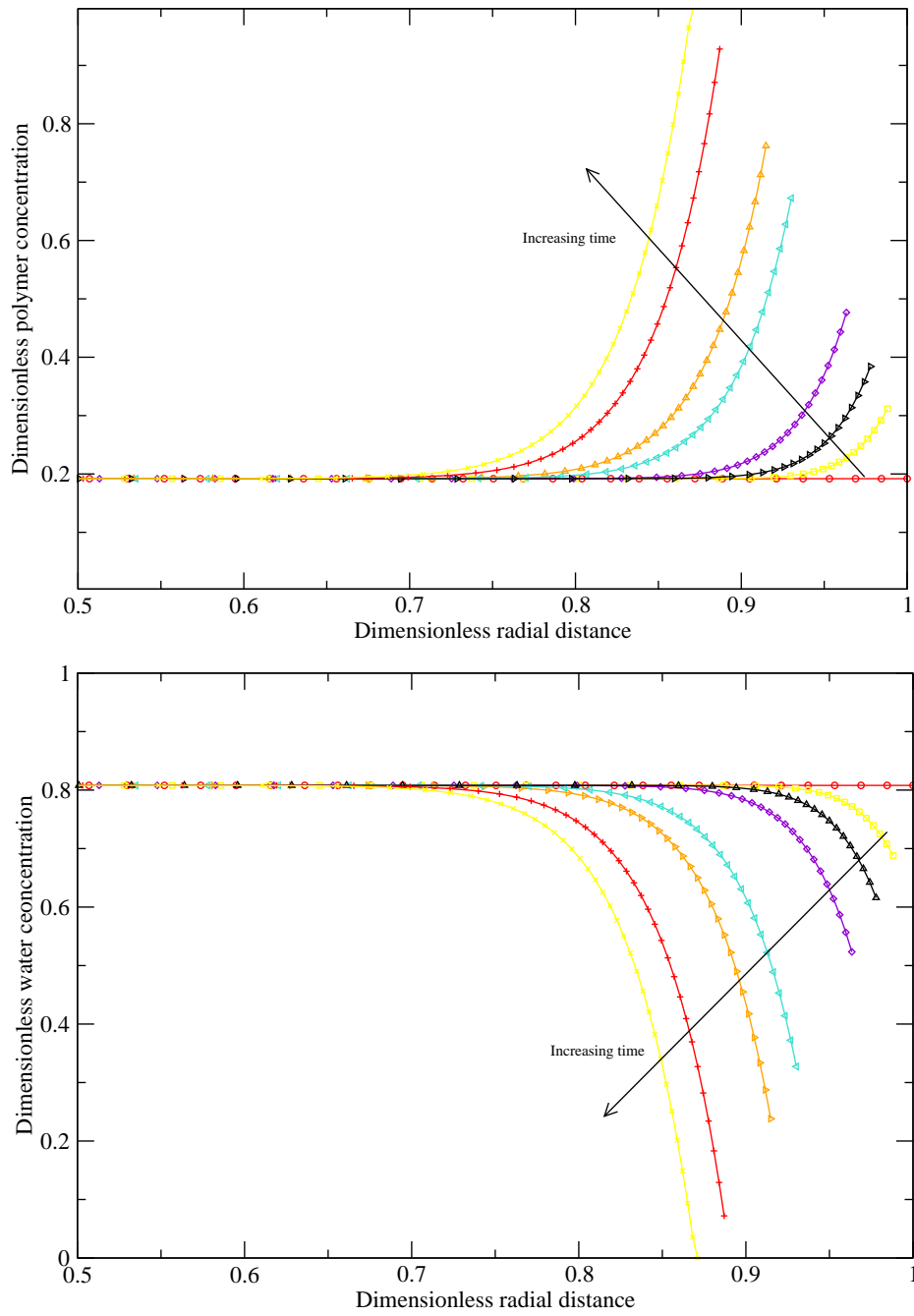


Figure 5: Spatial polymer (top) and water (bottom) profiles during the evaporation step. \circ : $\tau = 0.00$, \square : $\tau = 0.005$, \triangleright : $\tau = 0.0057$, \diamond : $\tau = 0.0063$, \triangleleft : $\tau = 0.0080$, \triangle : $\tau = 0.0087$, $+$: $\tau = 0.0102$, \times : $\tau = 0.0139$.

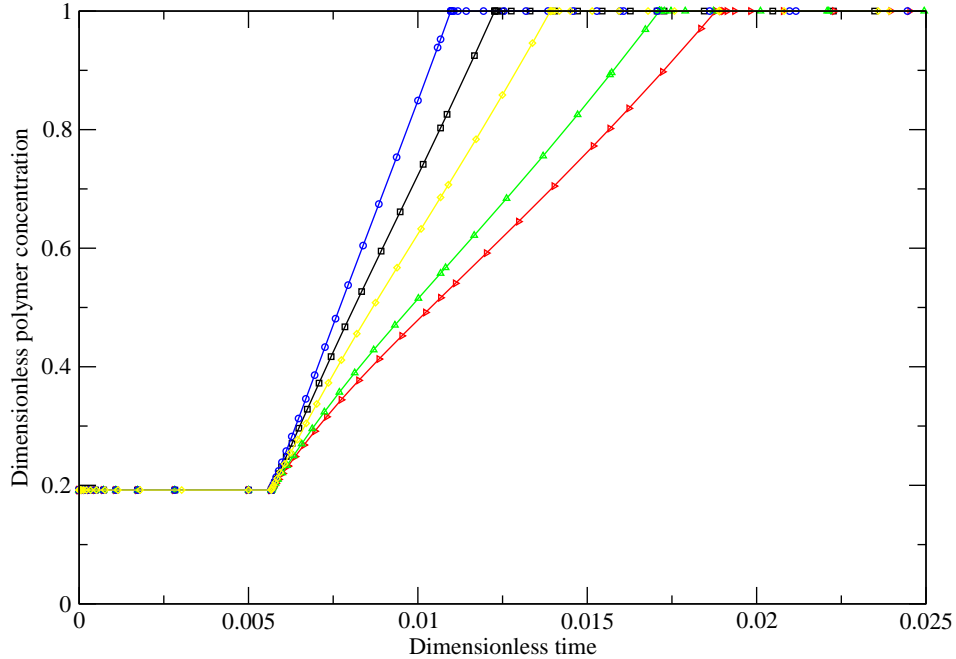


Figure 6: Polymer concentration profile at the surface to changes in the heat transfer coefficient. \circ : +25%, \square : +15%, \diamond : nominal, \triangle : -15%, and \blacktriangle : -25%.

temperature of air is made. The results are shown in Figure 9. The response shows that the time for skin formation varies inversely with increases in the inlet air temperature. The inlet air temperature determines the heat transfer rate to the droplet. Thus, an increase in the inlet air temperature increases the amount of heat transferred to the droplet. This leads to faster evaporation rates and therefore shorter times for skin formation.

6 Summary

A lab-scale experimental spray drying unit used for manufacturing polymeric hollow micro-particles has been described and a fundamental model that describes the mechanics of the formation of the hollow micro-particles starting from a single droplet was developed. The model, a system of nonlinear PDEs with a moving boundary, requires a numerical approach that follows the motion of the boundary accurately. The Gradient Weighted Moving Finite Elements method was chosen to solve this system of equations. The model was then used to predict the time to skin formation at the surface when parameter uncertainty and changes to the inlet operation conditions are present. The model predictions show that one can select the most appropriate conditions (temperatures and concentrations) and design a configuration to obtain hollow micro-particles with desirable properties.

Future work includes incorporating the curing reaction of the polymer. Currently, this is not a part of the model as the kinetics of the curing reaction are not known.

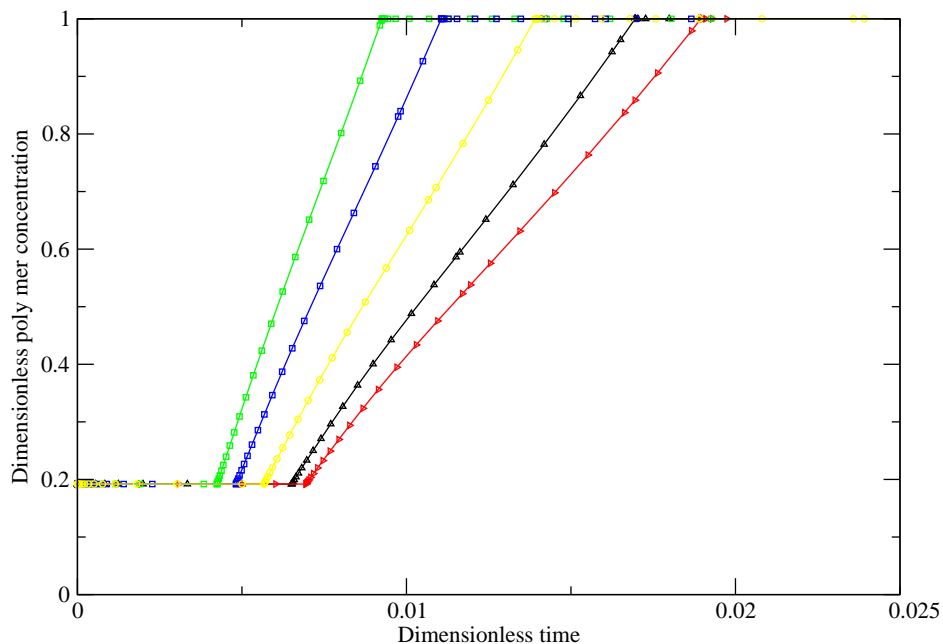


Figure 7: Polymer concentration profile at the surface for changes in the diffusivity coefficient. \circ : +25%, \square : +15%, \diamond : nominal, \triangle : -15%, and \triangleright : -25%.

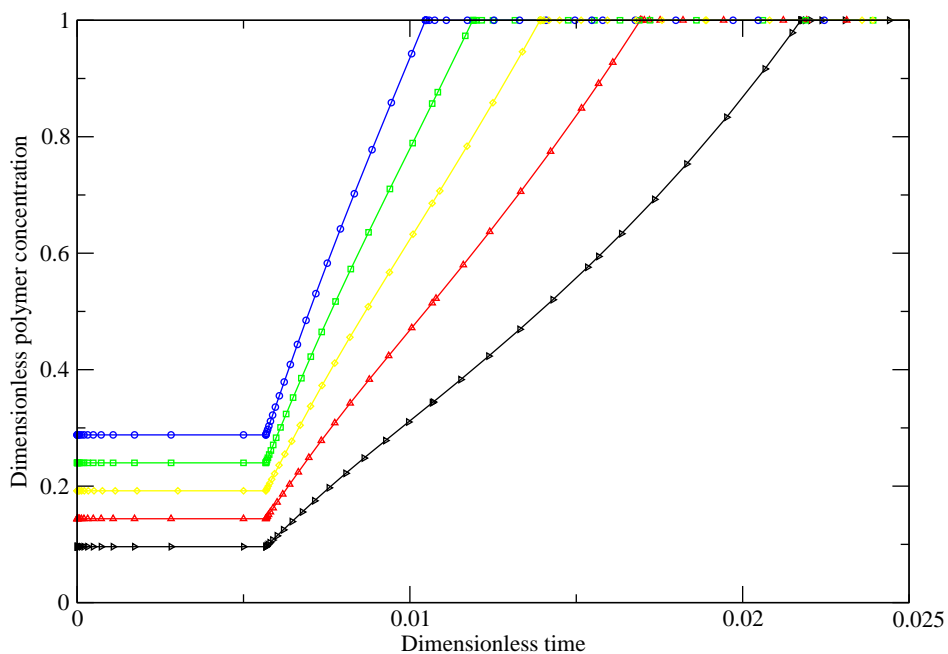


Figure 8: Polymer concentration profile at the surface for changes in the inlet feed concentration. \circ : +10%, \square : +5%, \diamond : nominal, \triangle : -5%, and \triangleleft : -10%.

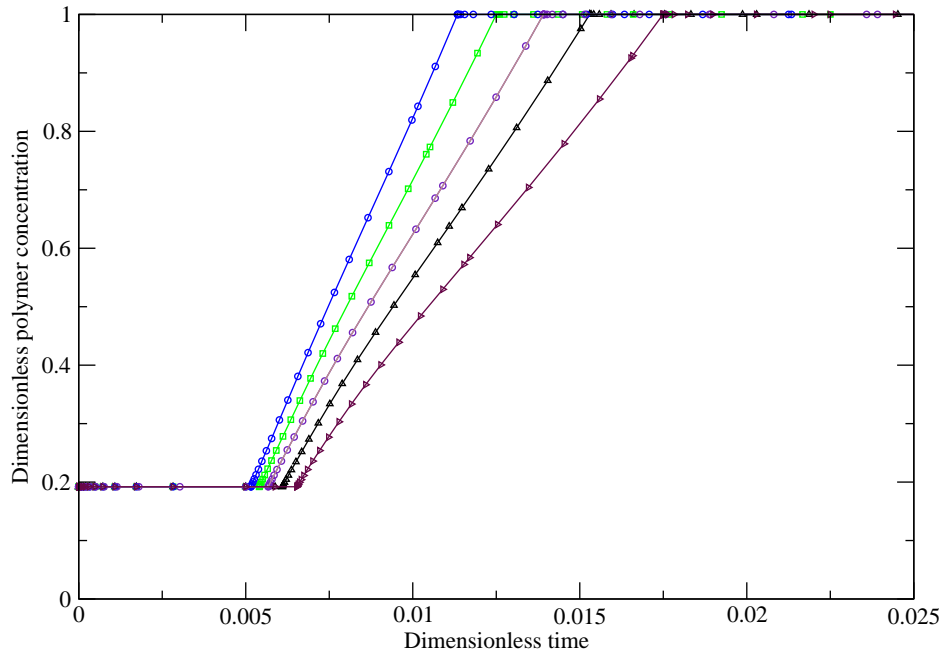


Figure 9: Polymer concentration profile at the surface for changes in the air temperature. \circ : $+50^{\circ}\text{C}$, \square : $+25^{\circ}\text{C}$, \diamond : nominal, \triangle : -25°C , and \blacktriangle : -50°C .

Acknowledgements

The first three authors were supported by Los Alamos National Laboratory, Los Alamos, NM. The experimental work and most of the computer simulations were done in the Chemical Engineering department at Texas Tech University. Most of the particle analysis was performed at the Los Alamos National Laboratory facilities in New Mexico.

Nomenclature

Bi_H	Biot number for heat transfer, dimensionless
C_p	Specific heat capacity of the solution, $\text{J kg}^{-1} \text{K}^{-1}$
H_{evap}	Dimensionless heat of vaporization
Le	Lewis number, dimensionless
M_P	Mass of polymer inside the droplet, kg
Nu	Nusselt number, dimensionless
Pr	Prandtl number, dimensionless
$R(0)$	Initial droplet radius, m
Re	Reynolds number, dimensionless
$R(t)$	Radius of the droplet at t s, m
Sc	Schmidt number, dimensionless
Sh	Sherwood number, dimensionless
T	Temperature of the droplet, K
T_0	The temperature of the droplet at $t = 0$ s
T_{air}	The inlet temperature of air, K
$T_l(r, 0)$	Initial local temperature, K
T_{sat}	Evaporation temperature of water, K
$X(\tau)$	Dimensionless radius
$c_{P,0}$	The initial polymer concentration in the droplet, kg m^{-3}
c_P	The concentration of polymer in the droplet at any time, kg m^{-3}
$c_{W,0}$	The initial water concentration in the droplet, kg m^{-3}
c_W	The concentration of water in the droplet at any time, kg m^{-3}
d_p	Droplet radius, m
h	External heat transfer coefficient, $\text{W m}^{-2}\text{K}$
k	Thermal Conductivity of the solution, $\text{W m}^{-1}\text{K}$
k_{air}	Thermal conductivity of air, $\text{W m}^{-1}\text{K}^{-1}$

k_x	Mass transfer coefficient, $m s^{-1}$
t	Time, s
t_0	Characteristic time, s
t_H	Time required for surface to reach evaporation temperature, s
v	Relative velocity of droplet, $m s^{-1}$
$x(\tau)$	Dimensionless radial distance
α	The thermal diffusivity of the solution
$\bar{c}_P(x, \tau)$	Dimensionless polymer concentration
$\bar{c}_W(x, \tau)$	Dimensionless water concentration
λ	Latent heat of vaporization, $J kg^{-1}$
\mathcal{D}	Binary diffusion coefficient of the water and polymer, $m^2 s^{-1}$
\mathcal{D}_{air}	Binary diffusion coefficient of the air and water, $m^2 s^{-1}$
r	Radial distance, m
μ	Viscosity of solution, Pa s
ρ_0	Initial solution density, $kg m^{-3}$
ρ	Density of solution, $kg m^{-3}$
ρ_W	Density of water, $kg m^{-3}$
τ	Dimensionless time
$\theta(x, \tau)$	Dimensionless temperature of the droplet

References

- [1] D. Wilcox and M. Berg. Microsphere fabrication and applications: an overview. Material Research Society, 1994.
- [2] K. Masters. *Spray Drying Handbook*. John Wiley and Sons., New York, NY, 1991.
- [3] Miller K. and Miller R. Moving finite elements, i. *Society for Industrial and Applied Mathematics journal on numerical analysis*, 18(7):1019–1032, 1981.
- [4] M. Vinjamur and R. Cairncross. Non-Fickian non-isothermal model for drying of polymer coatings. *AICHE J.*, 48:2444–2458, 2002.
- [5] B. Bird, W. Stewart, and E. Lightfoot. *Transport Phenomena*. John Wiley and Sons., New York, NY, 6th edition, 2002.
- [6] J. Prausnitz, B. Poling, and R. Reid. *Properties of gases and liquids*. McGraw-Hill, New York, NY, 4th edition, 1987.
- [7] R. Treybal. *Mass transfer operations*. McGraw-Hill, 3rd edition, 1980.
- [8] K. Miller. A geometrical-mechanical application of gradient weighted moving elements. *SIAM journal on numerical analysis*, 35:67–90, 1997.
- [9] P. Seydel, A. Sengespick, J. Blömer, , and J. Bertling. Experimental and mathematical modeling of solid formation at spray drying. *Chem. Eng. Tech.*, 27:505–510.
- [10] K. Miller and N. Carlson. Design and application of the gradient weighted moving finite element method in one dimension. *SIAM journal on numerical analysis*, 19:766–798, 1998.

Table 1: Dimensionless variables

Variable	Symbol	Definition
Dimensionless time	τ	$\frac{t}{t_0}$
Characteristic time	t_0	$\frac{R(0)^2}{\mathcal{D}}$
Dimensionless radial position	$x(\tau)$	$\frac{r(t)}{R(0)}$
Dimensionless droplet radius	$X(\tau)$	$\frac{R(t)}{R(0)}$
Dimensionless water concentration	$\bar{c}_W(x, \tau)$	$\frac{c_W(r, t)}{\rho_0}$
Dimensionless polymer concentration	$\bar{c}_P(x, \tau)$	$\frac{c_P(r, t)}{\rho_0}$
Dimensionless temperature	$\theta(x, \tau)$	$\frac{T(r, t) - T(r, 0)}{T_{air}(0) - T(r, 0)}$
Dimensionless Heat of vaporization	H_{evap}	$\frac{\lambda}{C_p(T_{air}(0) - T(r, 0))}$
Lewis number	Le	α/\mathcal{D}
Nusselt number	Nu	$\frac{h d_p}{k_{air}}$
Sherwood number	Sh	$\frac{k_x d_p}{c_W \mathcal{D}_{air}}$
Biot number	Bi_H	$\frac{h d_p}{k}$
Reynolds number	Re	$\frac{d_p v \rho}{\mu}$
Schmidt number	Sc	$\frac{\mu}{\rho \mathcal{D}_{air}}$
Prandtl number	Pr	$\frac{C_p \mu}{k}$

Table 2: Model parameter values

Parameter	Symbol	Value
Binary diffusion coefficient	\mathcal{D}	$1.25 \times 10^{-9} \text{ m}^2\text{s}^{-1}$
Mass transfer coefficient	k_x	1.265 ms^{-1}
Heat transfer coefficient	h	$1640 \text{ Wm}^{-2}\text{K}^{-1}$
Thermal diffusivity of water	α	$1.824 \times 10^{-7} \text{ m}^2\text{s}^{-1}$
Thermal conductivity of air	k_{air}	$0.0328 \text{ Wm}^{-1}\text{K}^{-1}$
Diffusion coefficient of air-water	\mathcal{D}_{air}	$0.375 \times 10^{-4} \text{ m}^2\text{s}^{-1}$
Reynolds number	Re	1.65×10^{-2} (dimensionless)
Schmidt number	Sc	2.5×10^{-2} (dimensionless)
Prandtl number	Pr	1.7 (dimensionless)